Determination of the efficiency of ethanol oxidation in a proton exchange membrane electrolysis cell

Rakan M. Altarawneh, Pasha Majidi and Peter G. Pickup*

Department of Chemistry, Memorial University, St. John's, Newfoundland, A1B 3X7, Canada

Submitted to Journal of Power Sources on 22 Dec 2016. Revised 9 Mar. Accepted 20 Mar 2017.

http://dx.doi.org/10.1016/j.jpowsour.2017.03.084

Abstract

Products and residual ethanol in the anode and cathode exhausts of an ethanol electrolysis cell (EEC) have been analyzed by proton NMR and infrared spectrometry under a variety of operating conditions. This provides a full accounting of the fate of ethanol entering the cell, including the stoichiometry of the ethanol oxidation reaction (i.e. the average number of electrons transferred per ethanol molecule), product distribution and the crossover of ethanol and products through the membrane. The reaction stoichiometry (n_{av}) is the key parameter that determines the faradaic efficiency of both EECs and direct ethanol fuel cells. Values determined independently from the product distribution, amount of ethanol consumed, and a simple electrochemical method based on the dependence of the current on the flow rate of the ethanol solution are compared. It is shown that the electrochemical method yields results that are consistent with those based on the product distribution, and based on the consumption of ethanol when crossover is accounted for. Since quantitative analysis of the cathode exhaust is challenging, the electrochemical method provides a valuable alternative for routine determination of n_{av}, and hence the faradaic efficiency of the cell.

Keywords: direct ethanol fuel cell; efficiency; crossover; product distribution; flow rate; number of electrons; stoichiometry

**Corresponding author. Tel.: 1-709-864-8657; Fax: 1-709-864-3702, E-mail:ppickup@mun.ca*

1. Introduction

The electrochemical oxidation of ethanol is of fundamental importance to the development of our understanding of organic electrocatalysis [1, 2] and has growing applications in energy technology [2-5] and sensors [6, 7]. Direct ethanol fuel cells [8, 9] (DEFC) offer the potential for efficient and clean energy production from biomass, while ethanol electrolysis [10-12] provides a renewable source of hydrogen for fuel cells. Electrochemical oxidation is widely used as an ethanol sensing mechanism in breath alcohol analyzers (breathalyzer).

In addition to measurement of electrochemical kinetics under a wide range of conditions, a full understanding of electrochemical ethanol oxidation requires knowledge of the stoichiometry (n_{av} = average number of electrons transferred per ethanol molecule) [13, 14], product distribution [13, 15, 16], and the nature and coverage of adsorbed intermediates [17-21]. Since the efficiency of a fuel cell or electrolysis cell is proportional to n_{av} [14], the reaction stoichiometry plays a critical role in the development of energy technologies based on electrochemical ethanol oxidation. It also influences the sensitivity of ethanol sensors, and variations in n_{av} with time and operating conditions will cause errors in breathalyzer measurements.

The complete oxidation of ethanol to carbon dioxide, which provides the highest theoretical energy efficiency for a fuel cell or electrolyzer, involves the transfer of 12 electrons as shown in equation 1.

$$CH_3CH_2OH + 3\ H_2O \rightarrow 2\ CO_2 + 12\ H^+ + 12\ e^- \qquad (1)$$

However, the main products formed during electrochemical oxidation are generally acetaldehyde (eq. 2) and acetic acid (eq. 3), which generate only 2 and 4 electrons, respectively.

$$CH_3CH_2OH \rightarrow CH_3CHO + 2\ e^- + 2\ H^+ \qquad (2)$$

$$CH_3CH_2OH + H_2O \rightarrow CH_3CO_2H + 4\ e^- + 4\ H^+ \qquad (3)$$

Ethyl acetate [22-25] from condensation of ethanol with the acetic acid, ethane [26], methane [26-28], ethane-1,1-diol [23, 25], ethoxyhydoxyethane [23, 25], and formic acid [29] have also been observed as minor products. In addition to greatly decreasing the energy efficiency of DEFCs and ethanol electrolyzers, the formation of acetaldehyde, acetic acid and other byproducts can decrease the effectiveness of both the anode and cathode catalysts, and has the potential to create significant environmental problems.

The efficiency of a DEFC (η_{cell}) is determined by the theoretical energy conversion efficiency (η_{rev}; thermodynamic efficiency), the voltage efficiency ($\eta_E = E_{cell}/E_{rev}$, where E_{cell} is the operating voltage and E_{rev} is the reversible cell potential), and the faradaic efficiency (η_F), according to eq. 4 [9, 15].

$$\eta_{cell} = \eta_{rev} \cdot \eta_E \cdot \eta_F \qquad (4)$$

The faradic efficiency is the ratio of the average number of electrons obtained per molecule of ethanol to the maximum of 12 for the complete oxidation to CO_2 ($\eta_F = n_{av}/12$), and is determined by the product distribution according to eq. 5 [16],

$$12 \cdot \eta_F = n_{av} = \sum n_i f_i \qquad (5)$$

where n_i is the number of electrons transferred to form product i and f_i is the fraction of ethanol converted to product i. Accurate use of eq. 5 requires all products to be identified and accurately quantified.

A recent analysis of low carbon power sources for vehicles has concluded that polymer electrolyte membrane (PEM) DEFCs, together with batteries, offer the best alternative to internal combustion engines [30]. However, this is based on the assumption that DEFCs that can operate at 50% efficiency will be developed, which will require n_{av} to be close to 12. Currently, the best efficiencies are ca. 11% for acid PEM DEFCs and ca. 23% for alkaline cells [9]. It has generally been found that increasing the electrochemical performance (voltage efficiency) of the anode

catalyst by combining Pt with other metals, such as Ru and Sn, in bi- and tri-metallic catalysts decreases the faradaic efficiency [4, 15, 31, 32]. However, in most cases, the faradaic efficiencies (or product distributions) of new catalysts have not been reported.

The development of better catalysts for ethanol fuel cells and electrolyzers [2-5] requires accurate methodologies for routine determination of n_{av}. Although it can be estimated from product distributions by use of eq. 5 [16], it has been shown that product analysis at the anode of a DEFC does not provide an accurate measure of the product distribution because of crossover of products through the membrane to the cathode, and chemical formation of products due to the crossover of ethanol and oxygen through the membrane [24, 31, 33]. Furthermore, accurate measurement of products exiting the cathode is difficult due to the high volatility of acetaldehyde [29] and condensation of acetic acid [33]. Although the effects of reaction with oxygen are not present in an electrolysis cell, analysis of products that crossover to the cathode remains a problem [33].

Previously, it has been shown that n_{av} for ethanol oxidation can be determined in DEFC hardware from the variation of the current (I) as a function of the flow rate (u) of the ethanol solution by use of eq. 6 [34].

$$I = n_{av} F C_{in} u \left(1 - \exp\left(- \frac{I_{lim}}{n_{av} F C_{in} u} \right) \right) \qquad (6)$$

where C_{in} is the concentration of ethanol entering the cell and I_{lim} is the limiting current at high flow rates. Although this equation was developed for a cell operating in crossover mode (Fig. 1A), the simplest configuration for development of the theory [35], it has subsequently been shown to also be valid for methanol oxidation in a normal electrolysis cell (anode polarization mode; Fig. 1B), and a model has been developed to account for losses due to crossover [35].

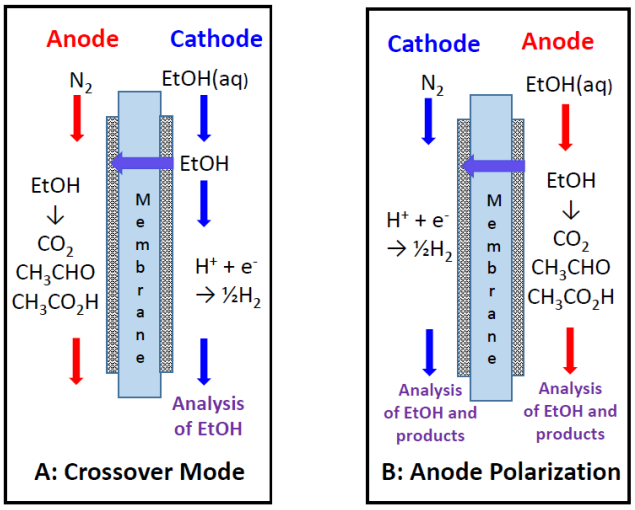

Figure 1. Schematic diagrams of the two cell configurations employed in this work.

The purpose of the work described here was to extend the use of eq. 6 to an ethanol electrolysis cell operating normally (i.e. in anode polarization mode), to verify its accuracy by measuring ethanol consumption and product distributions, and to assess the effects of ethanol crossover. Proton nuclear magnetic resonance (^{1}H-NMR) spectroscopy was used to measure the concentrations of acetaldehyde, acetic acid and residual ethanol exiting the cell, while CO_2 was analyzed with a commercial non-dispersive infra-red (NDIR) detector [36]. Analyses of the anode and cathode exhausts were performed separately in order to quantify the crossover of ethanol and products through the membrane. Previously, ^{1}H-NMR has been used to quantify products from ethanol oxidation with molecular catalysts [37], while solution and solid-state ^{13}C NMR have been used to identify and quantify ethanol and product distributions within and exiting a DEFC [23, 25], and in a cell with a liquid electrolyte [38].

This work was performed in an electrolysis cell rather than a DEFC in order to avoid the consumption of ethanol by chemical reaction with oxygen that would be supplied to the cathode in a DEFC. Accurate separation the effects of electrochemical and chemical oxidation of ethanol in a DEFC has not yet been achieved.

2. Experimental

2.1 The cell

Commercial fuel cell hardware (5 cm^2 active area; Fuel Cell Technology Inc.) was used for all electrochemical measurements. The anode inlet and both outlets of the cell were modified with stainless steel tubing that connected directly to the graphite flow field plates. The flow field channels were sealed with ethyl-2-cyanoacrylate [39] in order to minimize absorption of ethanol and reaction products into the graphite plates [33]. Membrane and electrode assemblies (MEA) were prepared by pressing (room temperature; ca. 1.5 MPa) two electrodes consisting of 4 mg cm^{-2} Pt black on Toray™ (TGP-H-090) carbon fiber paper onto a Nafion™ 115 membrane in the cell [40].

The two modes of operation employed are shown schematically in Fig. 1. In both cases, the cell was operated as an electrolysis cell, not a fuel cell. Measurements were made under steady state conditions at constant cell potentials using a Hokuto Denko HA-301 potentiostat. The flow rate of the 0.1 M ethanol (Commercial Alcohols Inc.) solution was controlled with a syringe pump. N_2 was passed through the anode (crossover mode) or cathode (anode polarization mode) at 9-32 mL min^{-1}. In both cases, the cathode reaction is $H^+ + e^- \rightarrow ½H_2$ and so the cathode acts a dynamic hydrogen electrode (DHE) and provides a relatively stable reference potential. The cell was operated at 50 ºC in initial experiments in order to achieve a suitable balance of products, limit ethanol crossover, and optimize the product collection procedure. It was then operated at 80 ºC to provide higher CO_2 yields and more stringent testing.

2.2 Ethanol and product analysis

For the experiment in crossover mode, the cathode solution was collected in a sealed vial cooled with ice. The residual ethanol concentration was determined by ^{1}H-NMR. The cell was operated at the selected fuel flow rate for at least 10 min before collecting a sample for analysis.

Analysis of products and residual ethanol when the cell was operated in anode polarization mode was complicated by crossover of all species though the membrane. In addition, the mixtures of gases (N_2 and CO_2) with volatile liquid components (acetaldehyde and ethanol) that are obtained make it difficult to obtain accurate analyses of all components [33]. Here, ^{1}H-NMR spectrometry was used to measure ethanol, acetic acid, and acetaldehyde separately in the anode and cathode exhausts, while CO_2 was determined in each exhaust by using a NDIR detector [36]. The experimental design shown schematically in Fig. 2 allowed residual ethanol and all products to be determined in both exhausts from a single experiment. CO_2 from the cathode (N_2 stream) was measured in real time with a Telaire 7001 CO_2 monitor following condensation of ethanol, water and products that had crossed the membrane in a 200 mL cold trap. The current and CO_2 readings were allowed to stabilize, and then averaged over a period of at least 100 s. The trap was cooled with ice, dry ice or liquid N_2 in the various experiments, but quantitative collection of acetaldehyde (boiling point 20 °C) was not achieved in most experiments. Use of liquid N_2 is complicated by condensation of the CO_2.

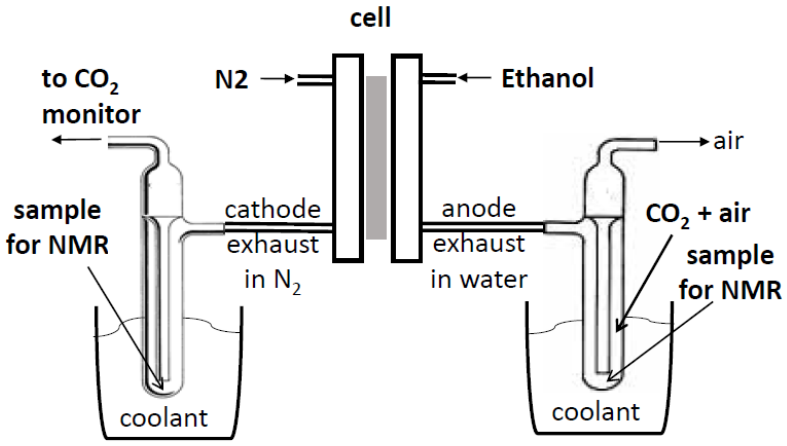

Figure 2. Schematic diagram of the product collection system employed in anode polarization experiments.

The anode exhaust solution was collected in a ca. 200 mL trap cooled with ice in the experiments at 50 °C and dry ice in the experiments at 80°C. At the end of each experiment, a sample of the solution was collected for analysis by ^{1}H-NMR, and then the CO_2 in the trap was flushed through the CO_2 monitor with N_2 at 9-35 mL min^{-1}. The CO_2 concentration was integrated until it reached the reading for the air initially in the trap.

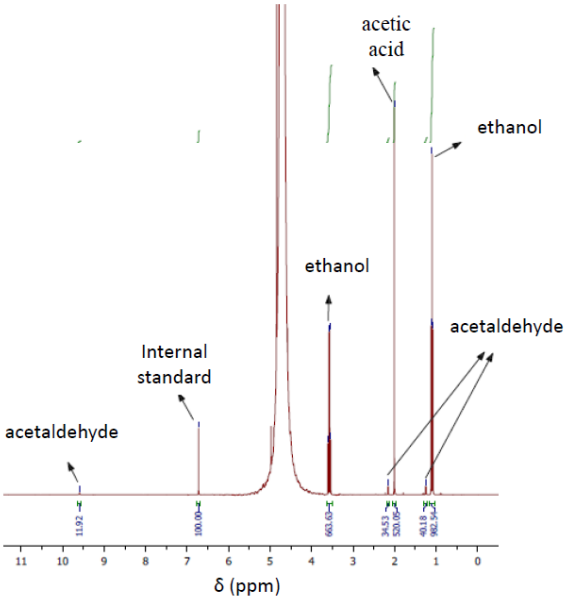

Figure 3. NMR spectrum of the anode exhaust solution from oxidation of 0.100 M ethanol at 0.7 V and 50 ºC in anode polarization mode.

For analysis by ^{1}H-NMR, 400 µL samples collected from the anode and cathode exhausts were mixed with 100 µL of D_2O containing 32 mM fumaric acid as an internal standard, which gives a singlet peak in the spectra at 6.72 ppm. Spectra were recorded on a Bruker AVANCE III 300 spectrometer. The D_2O in the sampled provided the field frequency lock and spectra were referenced to sodium 3-(trimethylsilyl)-2,2,3,3-tetradeuteropropionic propionate at 0 ppm. Fig. 3 shows an example of an NMR spectrum of a sample from the anode exhaust. The residual ethanol concentration was determined from the triplet at 1.10 ppm. The only products detected in

the exhaust solution were acetic acid (singlet at 2.01 ppm) and acetaldehyde (doublet at 2.15 ppm). Acetaldehyde forms a dimer under the conditions of these experiments [41], as indicated by the doublet at 1.24 ppm, and so the integral of this peak was included to give a single acetaldehyde concentration. Ethyl acetate was not detected.

Analysis of the cell exhausts was performed in triplicate at 0.2 mL min^{-1} only, since uncertainties became too large at higher and lower flow rates. This flow rate gave sufficient consumption of ethanol, while sample collection times were reasonable (to evaluate precision/reproducibility) and reasonably stable cell performances could be maintained.

3. Results and discussion

3.1. Operation of the cell in crossover mode

Initially, the cell was operated in crossover mode in order to develop the analytical methodology under well controlled mass transport conditions and without complications due to loss of ethanol due to crossover [35]. This allowed us to test the cell, and the assumptions made in the derivation of equation 6. These include the assumption of linear concentration gradients of ethanol across the membrane, that ethanol is quantitatively oxidized at the anode, and that the pressure drop across the membrane, concentration gradient in solution perpendicular to the flow direction, and lateral diffusion along the flow field are all negligible [34].

The cell was operated in the limiting current region at 0.7 V and 50 ºC (as demonstrated previously [34]) with ethanol solution supplied through the cathode flow field (negative electrode) so that it had to cross through the membrane to reach the anode, where it was electrochemically oxidized. N_2 was passed through the anode flow field to prevent interference from oxygen. Fig. 4 shows experimental data and theoretical (eq. 6) plots of current *vs.* fuel flow rate for 0.102 M ethanol supplied to the cathode. The best fit of the theoretical curve to the experimental data points was obtained with n_{av} = 4.43 and I_{lim} = 22.4 mA. These are within the

ranges previously reported for these conditions [34]. In order to check the assumption that all of the ethanol reaching the anode was being oxidized, the ethanol concentration in the solution exiting the cathode flow field was measured by NMR spectroscopy. Since ethanol should only cross the membrane or exit the cathode flow field, a discrepancy in the residual ethanol concentration would indicate that some ethanol reaching the anode was not oxidized, that one or more assumption were invalid, or that there were other losses (leakage) due to the hardware.

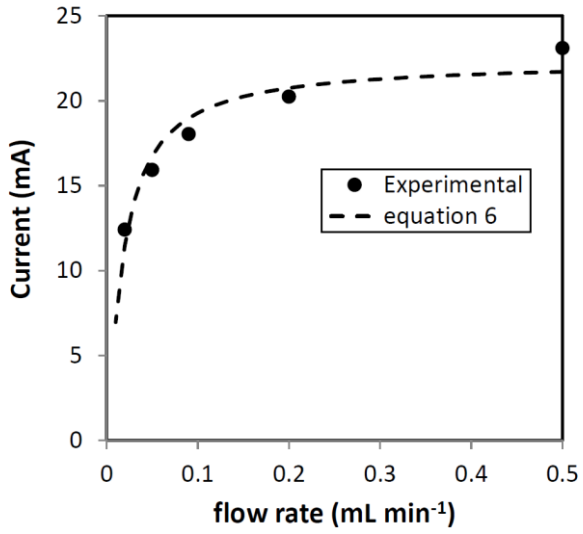

Figure 4. Current at 0.7 V *vs.* flow rate for oxidation of 0.102 M ethanol in crossover mode at 50 ºC (points) and best fit curve calculated by using eq. 6 with I_{lim} = 22.4 mA and n_{av} = 4.43.

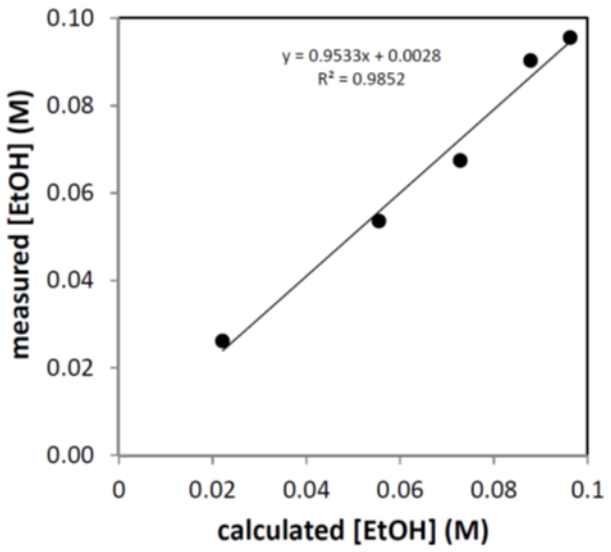

Figure 5. Experimental vs. calculated (eq. 7 with I_{lim} = 22.4 mA and n_{av} = 4.43) concentrations of ethanol exiting a cell under the conditions for Fig. 4.

Fig. 5 shows the measured concentrations of the residual ethanol content in the cathode exhaust (C_{out}) at different flow rates as a function of the expected ethanol exhaust concentrations calculated from eq. 7 [35] for I_{lim} = 22.4 mA and n_{av} = 4.43.

$$C_{out} = C_{in} \exp\left(-\frac{I_{lim}}{n_{av} F C_{in} u}\right) \qquad (7)$$

The good linearity of this plot (R^2 = 0.985) and slope (0.953) close to one indicates that the oxidation of ethanol at the anode was quantitative without significant loss of ethanol into the N_2 stream, and that the assumptions implicit in eq. 6 are reasonable. The uncertainties observed in Fig. 5 arise from a number of factors, including variations in n_{av} with flow rate, changes in the cell performance with time, and failure to reach a steady state concentration at the lowest flow rate because of the long time-scale required [34].

If it is assumed that ethanol was oxidized quantitatively in this experiment, and that there were no losses of ethanol, values of n_{av} can be obtained directly from the concentrations of ethanol in the cathode exhaust by using eq. 8.

$$n_{av} = I/uF(C_{in} - C_{out}) \qquad (8)$$

Application of this equation to the experimental data in Figs. 4 and 5 gave an average n_{av} of 4.4±0.7. The agreement of this value with that obtained from eq. 6 again indicates that losses of ethanol were not significant.

3.2. Operation of the cell in anode polarization mode

When operating the cell in anode polarization mode, an aqueous solution of 0.100 M ethanol was fed to the anode flow field, where ethanol is oxidized to generate electrons, protons, carbon dioxide, acetaldehyde, and acetic acid. This is the normal mode of operation of an ethanol electrolysis cell, and is also used to evaluate performances of anode catalysts and catalyst layers for DEFCs. Nitrogen was fed to the cathode flow field to avoid interference from oxygen and to provide a stable reference potential from the reduction of protons to hydrogen (DHE). The aim was to fully analyze the ethanol oxidation efficiency by determining n_{av}, accounting for any crossover losses, and complete accounting of the fate of ethanol consumption by analysis of the ethanol oxidation products.

3.2.1. Mass transport limited region: High current and low crossover

Fig. 6 shows polarization curves obtained in anode polarization mode at 50 °C and 80 °C with 0.100 M ethanol supplied to the anode. At 80 ºC the current reached a limiting value at 0.6 V. The slight decrease at 0.7 V can be attributed to a decrease in n_{av} (see below). At 50 ºC the current was at, or close to, the limiting value at 0.7 V. The increase in current when the temperature was increased is due to effects of temperature on the mass transport rate, electrochemical kinetics, and n_{av}.

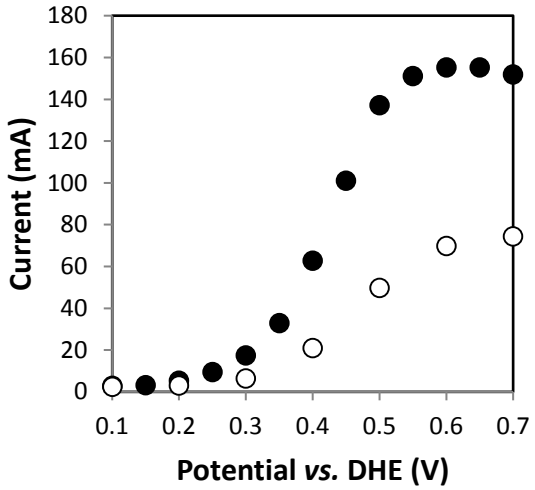

Figure 6. Polarization curves for oxidation of 0.100 M ethanol at 0.5 mL min^{-1} in anode polarization mode at 50 ºC (o) and 80 ºC (●).

Fig. 7 (□) shows the dependence of the experimental current at 0.7 V on the flow rate at 50 °C. The best fit theoretical curve (dashed line) from eq. 6 is also shown. It has previously been shown for methanol oxidation that eqs. 6 and 7 are both valid under these conditions [35]. The best fit parameters of n_{av} = 3.31 and I_{lim} = 83.7 mA are reasonable and so support the use of eq. 6 here. However, the central importance of n_{av} in determining the efficiencies of ethanol fuel cells and electrolysis cells makes it essential to know the accuracy of this methodology. To determine this, it is necessary to determine the product distribution, and ensure that all of the ethanol entering the cell is accounted for.

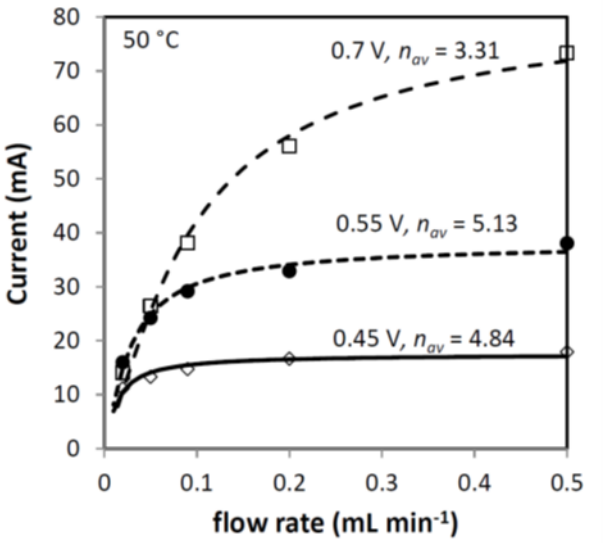

Figure 7. Current *vs.* flow rate for oxidation of 0.100 M ethanol at 50 ºC in anode polarization mode at 0.45 V (◊), 0.55 V (●), and 0.70V (□) with best fit curves calculated by using eq. 6 with I_{lim} = 17.5 mA and n_{av} = 4.84, I_{lim} = 38.2 mA and n_{av} = 5.13, and I_{lim} = 83.7 mA, n_{av} = 3.31, respectively.

Results of the chemical analysis of products and residual ethanol exiting the cell, obtained under the conditions used to determine n_{av} at 0.7 V in Fig. 7, are presented in the first row of Tables 1-3. Table 1 shows a comparison between the experimental and calculated ethanol exhaust concentrations (C_{out}) obtained by ^{1}H-NMR and based on the measured currents (eq. 7), respectively. It can be seen that only 1.3% of the ethanol entering the cell was detected in the cathode exhaust at 0.7 V, indicating that there was little crossover of ethanol at this potential. Under mass transport limited conditions, all of the ethanol entering the anode catalyst layer should have been oxidized before reaching the membrane [35]. The small amount of ethanol that was detected in the cathode exhaust may indicate that the cell was not quite at the mass transport limit (see Fig. 6), or may have been due to crossover through inactive regions of the MEA at the edges. The total ethanol measured in the cell exhaust at 0.7 V was somewhat higher than the

calculated value for n_{av} = 3.3±0.3, suggesting that n_{av} had been underestimated by use of eq. 6. Indeed, use of eq. 8 to calculate n_{av} from the amount of ethanol consumed yielded a value of 3.9±0.2.

T (°C)	Potential (V)	C_{out} (mM)			
		anode	**cathode**	**total**	**eq.7**
50	0.70	52±3	1.3±0.4	53±3	45.6
50	0.55	75±5	4.0±1.1	79±4	79.3
50	0.45	79±2	7.7±1.0	87±1	89.4
80	0.70	59.2±0.9	5.0±0.7	64.2±1.2	61.5
80	0.50	66±1	7.5±0.9	73.4±0.4	75.3
80	0.40	71±1	15.7±0.8	86.9±0.4	90.3

Table 1. Experimental (NMR) and calculated (eq. 7) concentrations of ethanol exiting a cell operating in anode polarization with 0.100 M ethanol supplied to the anode at 0.2 mL min^{-1}. Averages and standard deviations for three consecutive experiments are presented.

The measured product distribution for these experiments at 0.7 V (Table 2) clearly demonstrates the effects of crossover [33], and also shows a poor mass balance. Similar amounts of CO_2 were measured in the anode and cathode exhausts, showing that there was facile crossover of CO_2 to the cathode. The chemical yield of CO_2 was 7.6% from the combined analyses. In contrast, there was much less crossover of acetic acid, with only 4.4% of the total chemical yield of 62% appearing at the cathode. This can be attributed to the low volatility of acetic acid [33]. Acetaldehyde was also predominantly observed at the anode, although in this case the anode to cathode ratio does not accurately reflect the amount of crossover, since the low

mass balance ("sum" column in Table 2) can be attributed primarily to inefficient collection of acetaldehyde from the cathode gas stream [33]. This was confirmed by later experiments (below) in which the acetaldehyde collection efficiency was improved.

T	potential	%CO_2		%Acetic acid		%acetaldehyde		sum*	n_{av}
(°C)	(V)	anode	Cathode	anode	cathode	anode	cathode		
50	0.70	4.2 ±0.3	3.4±0.1	59±6	2.7±0.2	8.9±0.6	0.3±0.2	78±7%	4.0±0.2
50	0.55	6.2±1.4	4.5±0.4	53±2	13±3	13±6	1.9±0.8	92±8%	4.4±0.2
50	0.45	8.0±0.7	5.1±0.5	27.2±0.4	7.1±0.6	27±6	6.9±1.5	81±8%	4.0±0.1
80	0.70	13.3±0.4	10.6±0.9	36±2	11.9±0.4	6.0±1.2	2.6±0.3	80±3%	5.3±0.1
80	0.50	18.6±0.6	11.9±0.1	39±2	14.1±0.6	8.5±0.9	3.7±0.3	96±1%	6.1±0.1
80	0.40	26.8±1.4	8.8±0.3	33±4	16.6±0.8	9.9±1.4	4.8±0.8	100±5%	6.6±0.2

* the mass balance varies due to variations in the acetaldehyde collection efficiency.

Table 2. Summary of chemical analysis results for the anode and cathode exhausts of a cell operating in anode polarization mode with 0.100 M ethanol at a flow rate of 0.2 mL min^{-1}. Chemical yields are given, based the measured quantities of products and the amount of ethanol consumed. Averages and standard deviations for three consecutive experiments are presented.

The chemical yields of CO_2 and acetic acid given in Table 2 were used to estimate n_{av} by using eq. 5. Since the measured acetaldehyde yield was known to be inaccurate, a value estimated by mass balance ($f_{carbon\ dioxide} + f_{acetic\ acid} + f_{acetaldehyde} = 1$) was used. This gave n_{av} = 4.0±0.2, while use of the measured acetaldehyde yield (i.e. assuming that C_{out} was inaccurate) gave n_{av} = 3.6±0.4, which was not statistically different.

T (°C)	Potential (V)	CO_2 yield	acetic acid yield	acetaldehyde yield from charge balance	n_{av}
50	0.70	24±1%	63±4%	13±5%	4.1±0.2
50	0.55	27±2%	57±6%	15±5%	4.1±0.2
50	0.45	41±1%	36±2%	24±1%	4.15±0.01
80	0.70	53±2%	35±1%	12±2%	5.2±0.2
80	0.50	61±2%	35±1%	4±3%	6.3±0.1
80	0.40	66±1%	31±1%	3.0±0.8%	6.8±0.1

Table 3. Faradaic yields for CO_2, acetic acid and acetaldehyde from a cell operating in anode polarization mode with 0.100 M ethanol at a flow rate of 0.2 mL min^{-1}. CO_2 and acetic acid yields are based on the combined analyses from the anode and cathode. Averages and standard deviations for three consecutive experiments are presented.

Because of the difficulty in obtaining accurate acetaldehyde analyses, and the expectation that the faradaic yields of CO_2 and acetic acid obtained by NDIR and ^{1}H-NMR were accurate, n_{av} values were also determined from the CO_2 and acetic acid analyses and the charge balance. Faradaic yields (F_i) are presented in Table 3 together with n_{av} calculated by using eq. 9.

$$n_{av} = 12/(F_{carbon\ dioxide} + 3F_{acetic\ acid} + 6F_{acetaldehyde}) \quad (9)$$

The n_{av} of 4.1±0.2 calculated in this way is not statistically different from the value in Table 2 based on the mass balance. Consequently it can be concluded that failure to obtain a quantitative analysis of the acetaldehyde produced by the cell does not significantly compromise the accuracy of n_{av}. A summary of the n_{av} values obtained by the various procedures is given in Table 4, where it can be seen that there is very good agreement between the values from eqs. 5, 8 and 9 (*t* tests show that the differences were not significant). However, eq. 6 significantly underestimated

n_{av} in this case, which can be attributed to a systematic error due to a slow decrease in the cell performance over the course of the experiment.

Mode	T (°C)	Potential (V)	n_{av}			
			***i* vs. *u* (eq. 6)**	**ethanol consumed (eq. 8)**	**faradaic yields (eq. 9)**	**chemical yields (eq. 5)**
Crossover	50	0.70	4.4±0.2	4.4±0.7	*	*
Anode pol.	50	0.70	3.3± 0.3	3.9±0.2	4.1±0.2	4.0±0.2
Anode pol.	50	0.55	5.1±0.2	4.7±0.4	4.1±0.2	4.4±0.2
Anode pol.	50	0.45	4.8±0.2	3.8±0.2	4.15±0.01	4.0±0.1
Anode pol.	80	0.70	5.6±0.3	5.4±0.2	5.2±0.2	5.3±0.1
Anode pol.	80	0.50	7.0±0.1	6.0±0.1	6.3±0.1	6.1±0.1
Anode pol.	80	0.40	7.7±0.2	6.5±0.3	6.8±0.1	6.6±0.2

* not determined

Table 4. Summary of n_{av} values obtained in this work.

When the temperature of the cell was raised to 80 °C, the current at 0.7 V increased significantly (Fig. 6), while the amount of ethanol consumed decreased (Table 1). The increased current and efficiency are consistent with the higher n_{av} (5.55 at 80 °C vs. 3.31 at 50 °C) obtained by fitting the currents to eq. 6. A similar difference in the ethanol consumed is obtained from eq. 7 (Table 1). The product analyses at 80 °C also show an increase in the efficiency for ethanol oxidation to CO_2 (Tables 2 and 3), with n_{av} increasing to 5.2-5.3, which is consistent

with the values of 5.6±0.3 and 5.4±0.2 from eqs. 6 and 8, respectively (Table 4). The increased CO_2 yield at 80 °C *vs.* 50 °C is consistent with literature reports (see Table 5). It can also be seen from the data in Table 1 that there was considerably more crossover of ethanol to the cathode at 80 °C relative to 50 °C.

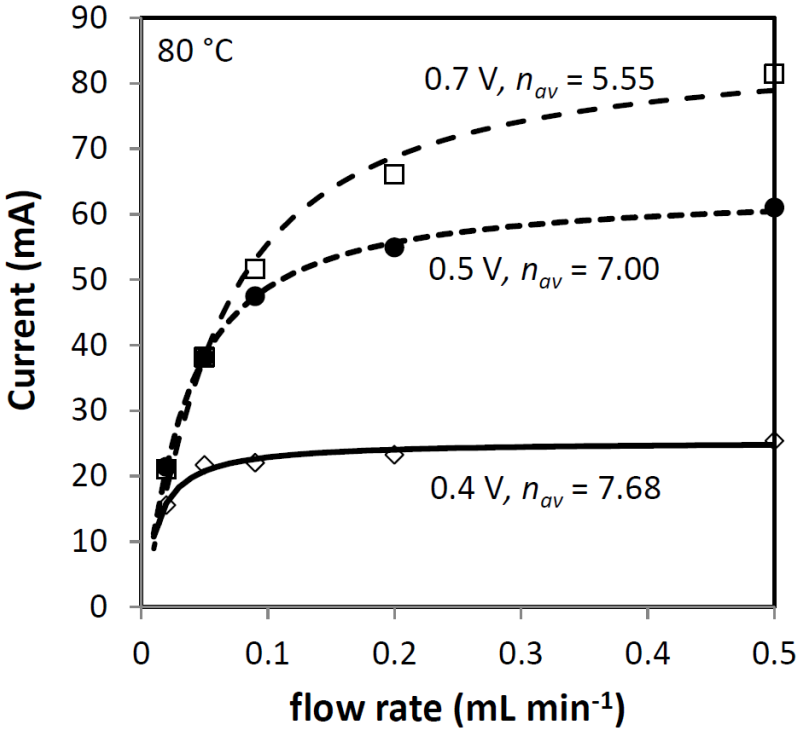

Figure 8. Current *vs.* flow rate for oxidation of 0.100 M ethanol at 80 ºC in anode polarization mode at 0.4 V (◊), 0.50 V (●), and 0.70 V (□) with best fit curves calculated by using eq. 6 with I_{lim} = 25.3 mA and n_{av} = 7.68, I_{lim} = 63.9 mA and n_{av} = 7.00, and I_{lim} = 86.8 mA, n_{av} = 5.55, respectively.

3.2.2. Low current region with crossover

Experiments were also performed at potentials below the mass transport limited region in order to explore the use of eq. 6 to determine n_{av} under the mixed kinetic and mass transport conditions employed in fuel cells and electrolysis cells. Under these conditions, the concentration

of ethanol does not drop to zero at the anode-membrane interface, and this results in crossover of ethanol to the cathode [35]. Since, the derivation of eqs. 6 and 7 assumes that all of the ethanol reaching the anode is oxidized [34], loss of ethanol by crossover would be expected to result in errors. Indeed, this was observed for methanol oxidation at potentials below the limiting current region, and the model was adapted in order to account for and quantify crossover [35]. Here, the loss of ethanol into the cathode exhaust was quantified by NMR and current *vs.* flow rate data were analyzed by using both models (eq. 6 and a finite difference simulation with crossover) to assess the influence of ethanol crossover. n_{av} values from product analyses were used to assess the accuracy of the n_{av} values obtained from analysis of *I vs. u* curves.

Fig. 7 (●) shows current as a function of flow rate at 50 °C for an experiment at 0.55 V, which provided only 46% of the current at 0.7 V. Fitting of these data to eq. 6 gave n_{av} = 5.13 and I_{lim} = 38.2 mA. The measured ethanol exhaust concentrations are given in row 2 of Table 1, where it can be see that there was significant crossover of ethanol to the cathode. Approximately 4% of the ethanol entering the cell was detected in the cathode exhaust, which corresponds to 19% of (C_{in} - $C_{out\text{-}T}$), where $C_{out\text{-}T}$ is the sum of the ethanol concentrations in the anode ($C_{out\text{-}A}$) and cathode ($C_{out\text{-}C}$) exhausts. C_{out} calculated with eq. 7 was 79.3 mM for n_{av} = 5.13, which agrees well with the experimental total ($C_{out\text{-}T}$) of 79 mM.

In order to investigate whether the crossover of ethanol caused an error in the n_{av} obtained from eq. 6, the experimental *I vs. u* and $C_{out\text{-}A}$ data were fitted to the simulation [35] that includes a crossover parameter. The best fit gave n_{av} = 5.19 and I_{lim} = 39.2 mA, and 4.8% loss of ethanol due to crossover. The crossover loss from the simulation agrees well with the experimental value of 4.0±1.1%, while the insignificant change in n_{av} shows that this small amount of crossover does not compromise the accuracy of eq. 6. I_{lim} was increased slightly in the simulation because it is the limiting current that would be observed in the absence of crossover.

Full product analysis for the anode and cathode exhausts was used to test the accuracy of the n_{av} of 5.1±0.2 obtained from *I vs. u*, and the results are shown in row 2 of Tables 2 and 3. The analysis provided a good mass balance, with n_{av} = 4.4±0.2 (Table 2), which agreed within the experimental uncertainty with the n_{av} of 4.1±0.2 from the faradaic yields of CO_2 and acetic acid (Table 3). Equation 7, based on the amount of ethanol consumed, gave a similar value of 4.7±0.4. The reasonable agreement of all of these n_{av} values indicates that eq. 6 provides a useful measure of n_{av} under these conditions.

Fig. 7 (◊) shows current as a function of flow rate for an experiment at 0.45 V, which provided only 21% of the current at 0.7 V. Fitting of these data to eq. 6 gave n_{av} = 4.84 and I_{lim} = 17.5 mA, and use of these parameters in eq. 7 gave C_{out} = 89.4 mM at 0.2 mL min^{-1}. The exhaust concentrations are given in row 3 of Table 1, where it can be see that there was increased crossover of ethanol to the cathode relative to the experiments at 0.55 V and 0.7 V. The measured $C_{out\text{-}T}$ was slightly higher than the value from eq. 7, suggesting that the n_{av} of 4.84 may have been slightly overestimated by use of eq. 6. Indeed, calculation of n_{av} from the amount of ethanol consumed (eq. 8) gave a lower value of 3.8±0.2. This conjecture was supported by analysis of the products, which provided n_{av} = 4.0±0.1 based on the mass balance (Table 2) and n_{av} = 4.15±0.01 based on the charge balance (Table 3).

It should be noted that n_{av} values obtained from the flow rate dependence of the current (eq. 6) represent averages over the range of flow rates employed, and should not necessarily match those measured from ethanol and product analysis at a specific flow rate. Since the CO_2 yield increases with decreasing ethanol concentration, and the average concentration of ethanol in the flow field decreases with decreasing flow rate, n_{av} increases with decreasing flow rate [34]. In the experiments at 0.45 V, the average ethanol concentration in the anode flow field was ca.

89 mM at 0.2 mL min^{-1}, but only 80 mM over the range of 0.02 to 0.5 mL min^{-1}. This can adequately explain the higher n_{av} from eq. 6.

In order to assess the effect of crossover on the n_{av} from eq. 6, the experimental *I vs. u* and $C_{out\text{-}A}$ data at 0.45 V were fitted to the simulation with crossover. The best fit gave n_{av} = 4.98, I_{lim} = 18.6 mA, and 10.4% loss of ethanol due to crossover. The measured loss due to crossover was 7.7±1.0%, and so again the value from the simulation is reasonable. The slightly higher n_{av} from the simulation relative to eq. 6 should be more accurate, although the difference is not statistically significant.

Current vs flow rate data at 80 °C for two potentials (0.4 and 0.5 V) below the mass transport controlled region are shown in Fig. 8. Fitting of eq. 6 to these data sets gave n_{av} = 7.68 at 0.4 V and n_{av} = 7.00 at 0.5 V, which are both significantly higher than the value of 5.55 obtained at 0.7 V. This decreasing n_{av} with increasing potential is consistent with literature reports [42, 43], as are the higher values relative to those obtained at 50 °C (Table 4). Analysis of the ethanol (Table 1) and products (Tables 2 and 3) exiting the cell gave somewhat lower n_{av} values than eq. 6, as can been seen from the summaries in Table 4. This can be attributed to the effect of flow rate on n_{av}. The ethanol exhaust concentrations in Table 1 indicate that ca. 15.7% and 7.5% of the ethanol entering the cell crossed over to the cathode at 0.4 V and 0.5 V, respectively. Simulations show that these levels of crossover would make n_{av} values from eq. 6 ca. 2-5% too low.

3.3 Discussion

It is clear from the results in Table 4 that all four methods for determining n_{av} give similar results under a variety of conditions. There are significant uncertainties in all cases, and there may be some systematic errors. Crossover of ethanol would be expected to cause an error when eq. 6 is used, although modelling of this indicates that it was not a significant source of error (<

5%) here. Loss of acetaldehyde during sample collection would also lead to a systematic error, but this has been accounted for by using the mass and charge balances. n_{av} values obtained from the mass and changes balances did not differ significantly, indicating good accuracy.

From inspection of the results in Table 4, it can be seen that the flow rate dependence of the current (eq. 6) provides a valuable method for routine determination of n_{av}. It can be applied as a simple extension of a polarization experiment, and can track changes in the stoichiometry as the operating conditions (e.g. T, C_{in}, pressure) of the cell are changed. In combination with a simple, inexpensive, commercial CO_2 detector, it can provide the product distribution from eq. 9 with charge balance, if it is assumed that the only products are CO_2, acetic acid and acetaldehyde. A conductivity sensor can also be employed to monitor acetic acid production [44]. Where necessary, the results can be verified and refined by analysis of the combined exhaust solutions by NMR or chromatography. The product distribution and n_{av} can be obtained from just the ethanol and acetic acid concentrations by applying eq. 8 to obtain n_{av} and solving eq. 5 with mass balance. This simplifies the analytical procedure considerably, and potential errors due to the loss of ethanol into the gas stream can be avoided if the CO_2 does not need to be measured.

We have applied eq. 6 and the comprehensive analysis methodology reported here to a DEFC (i.e. with air at the cathode), but have not achieved a satisfactory accounting of the crossover effects and production of CO_2, acetic acid and acetaldehyde by the chemical reaction of ethanol with oxygen. Although comprehensive analysis of the products and residual ethanol should provide this information, changes in the current and product distributions with time produced unacceptable uncertainties. Consequently, the anode polarization data presented here provide the best estimates available for the stoichiometry and product distribution of ethanol oxidation in a DEFC.

The n_{av} values reported in Table 4 and product distributions reported in Tables 2 and 3 are consistent with literature reports, and follow similar trends. Representative product distributions from the literature are presented in Table 5, together with n_{av} for each distribution calculated with eq. 5 for chemical yields or eq. 9 for faradaic yields. Where only the CO_2 yield was reported, the range of n_{av} given is for 0% acetic acid to 0% acetaldehyde. At 50 °C, the literature n_{av} values range from 2.1 to 4.2, while those in Table 4 range from 3.3 to 5.1. The higher values in this work, which are due to the higher CO_2 yields (Table 3), can be attributed to the use of a high loading of Pt black (4 mg cm^{-2}) compared with low loadings of 20% Pt on carbon (0.028 to 0.04 mg cm^{-2}) in the literature reports [16, 42]. At 80 °C, the literature n_{av} values range from 2.6 to 7.3 while those in Table 4 range from 5.2 to 7.7, again showing good compatibility in light of the high Pt loading and low ethanol concentration employed here. The n_{av} values in Table 5 are generally much higher at 80 °C than 50 °C, as found in this work (Table 4).

Generally, it can be seen from the data in Table 5 that the CO_2 yield decreases as the anode potential is increased, and the results in Table 4 also follow this trend. This can be attributed to the effect of oxide formation on the Pt surface, which is necessary to oxidize the adsorbed CO intermediate, but restricts the number of contiguous site available for ethanol adsorption [42, 45]. Consequently, for efficient oxidation of ethanol, it is important to avoid oxide formation on Pt. This requires a second, oxophilic component, such as Ru or Sn, to provide the oxide required to form CO_2 at lower potentials [32, 46, 47]. However, since the dissociation of the C-C bond of ethanol requires 3 adjacent Pt sites [48, 49], the presence of a second metal on the Pt surface can inhibit dissociation and causes a decrease in CO_2 formation. Consequently, the surface coverage of the second metal must be low, or it should be present as a separate phase. Oxide supports can provide the required oxide sites and have been shown to increase activities

while maintaining high efficiency for the complete oxidation [50-56]. It is an approach that offers great potential for the development of efficient DEFCs. However, further work is required in order to establish that oxide supported catalysts produce high stoichiometries under fuel cell conditions.

T (°C)	**catalyst**	**Pt loading (mg cm^{-2})**	**[EtOH] (M)**	**potential (V) *reference*[a]**	**yield[b]**			***n_{av}***	**ref.**
					%AL	**%AA**	**%CO_2**		
50	20% Pt/C	0.028	0.1	scan	37	60	2.7	3.0	[16]
50	20% Pt/C	0.04	0.1	0.48 *RHE*	-	-	7.8	2.1-4.2	[42]
80	20% Pt/C	0.04	0.1	0.48 *RHE*	-	-	25.7	2.55-4.83	[42]
80	60% Pt/C	3.0	2.0	-0.4 to -0.6 *cathode*	47.5	32.5	20	4.7	[15]
80	Pt black	4.0	0.5	-	41.9	39.5	18.6	3.09	[44]
80	Pt black	4.0	0.1	0.4 *DHE*	-	-	56	3.8-6.8	[57]
80	63% Pt/C	1.0	0.5	-0.1 *cathode*	*14*	*65*	*21*	5.4	[31]
80	63% Pt/C	1.0	0.5	-0.2 *cathode*	*29*	*57*	*14*	4.6	[31]
80	18% Pt/C	1.0	0.2	-0.1 *cathode*	*15*	*47*	*37*	6.7	[58]
80	18% Pt/C	1.0	0.2	-0.2 *cathode*	*21*	*31*	*47*	7.3	[58]

a. *cathode* is the oxygen electrode of a fuel cell

b. faradaic or *chemical* (italics) yields

- not reported

Table 5. Summary of product yields and calculated n_{av} values from literature reports of ethanol oxidation at 50 °C and 80 °C. AL is acetaldehyde, AA is acetic acid.

4. Conclusions

The flow rate dependence of the current for a fuel cell operated in anode polarization mode can provide a good estimate of the stoichiometry (n_{av}) of ethanol oxidation at a DEFC anode, or in a PEM electrolysis cell. Errors due to crossover are typically < 5%. The stoichiometry can also be conveniently obtained from analysis of the ethanol in the anode and cathode exhausts by NMR, which also provides the rate of crossover of ethanol through the membrane. NMR analysis also provides the yield of acetic acid, which allows the yields of acetaldehyde and CO_2 to be estimate from n_{av}. This is important because of the experimental difficulty of quantitative collection of the acetaldehyde. Furthermore it will be important in the determination of product distributions from DEFCs where the chemical reaction of ethanol with oxygen also produces acetaldehyde, acetic acid, and CO_2.

Acknowledgements

This work was supported by the Natural Sciences and Engineering Research Council of Canada and Memorial University.

References

[1] M.T.M. Koper, S.C.S. Lai, E. Herrero, Mechanisms of the oxidation of carbon monoxide and small organic molecules at metal electrodes in: Fuel Cell Catalysis, John Wiley, 2009, pp. 159-207.

[2] Y. Wang, S.Z. Zou, W.B. Cai, Catalysts, 5 (2015) 1507-1534.

[3] E. Antolini, J. Power Sources, 170 (2007) 1-12.

[4] J. Friedl, U. Stimming, Electrochim. Acta, 101 (2013) 41-58.

[5] M.A.F. Akhairi, S.K. Kamarudin, Int. J. Hydrogen Energy, 41 (2016) 4214-4228.

[6] J.G. Wigmore, R.M. Langille, Can. Soc. Forensic Sci. J., (2009) 276-283.

[7] M.R. Rahman, J.T.S. Allan, M.Z. Ghavidel, L.E. Prest, F.S. Saleh, E.B. Easton, Sensors and Actuators B-Chemical, 228 (2016) 448-457.

[8] S.P.S. Badwal, S. Giddey, A. Kulkarni, J. Goel, S. Basu, Applied Energy, 145 (2015) 80-103.

[9] L. An, T.S. Zhao, Y.S. Li, Renew. Sustain. Energy Rev., 50 (2015) 1462-1468.

[10] V. Bambagioni, M. Bevilacqua, C. Bianchini, J. Filippi, A. Lavacchi, A. Marchionni, F. Vizza, P.K. Shen, ChemSusChem, 3 (2010) 851-855.

[11] C. Lamy, T. Jaubert, S. Baranton, C. Coutanceau, J. Power Sources, 245 (2014) 927-936.

[12] A.R. de la Osa, A.B. Calcerrada, J.L. Valverdea, E.A. Baranova, A. de Lucas-Consuegra, Appl. Catal., B Env., 179 (2015) 276-284.

[13] H. Hitmi, E.M. Belgsir, J.M. Leger, C. Lamy, R.O. Lezna, Electrochim. Acta, 39 (1994) 407-415.

[14] F. Vigier, C. Coutanceau, A. Perrard, E.M. Belgsir, C. Lamy, J. Appl. Electrochem., 34 (2004) 439-446.

[15] S. Rousseau, C. Coutanceau, C. Lamy, J.M. Leger, J. Power Sources, 158 (2006) 18-24.

[16] H. Wang, Z. Jusys, R.J. Behm, J. Phys. Chem. B, 108 (2004) 19413-19424.

[17] B. Beden, M.C. Morin, F. Hahn, C. Lamy, J. Electroanal. Chem., 229 (1987) 353-366.

[18] T. Iwasita, W. Vielstich, J. Electroanal. Chem., 257 (1988) 319-324.

[19] F. Vigier, C. Coutanceau, F. Hahn, E.M. Belgsir, C. Lamy, J. Electroanal. Chem., 563 (2004) 81.

[20] D.M. dos Anjos, F. Hahn, J.M. Leger, K.B. Kokoh, G. Tremiliosi, J.M. Feliu, E. Herrero, P. Waszczuk, A. Crown, S. Mitrovski, A. Wieckowski, J. Solid State Electrochem., 11 (2007) 1567–1573.

[21] A.B. Delpeuch, F. Maillard, M. Chatenet, P. Soudant, C. Cremers, Appl. Catal., B Env., 181 (2016) 672-680.

[22] Q. Wang, G.Q. Sun, L. Cao, L.H. Jiang, G.X. Wang, S.L. Wang, S.H. Yang, Q. Xin, J. Power Sources, 177 (2008) 142-147.

[23] Y. Paik, S.S. Kim, O.H. Han, Electrochem. Commun., 11 (2009) 302-304.

[24] A. Jablonski, P.J. Kulesza, A. Lewera, J. Power Sources, 196 (2011) 4714–4718.

[25] I. Kim, O.H. Han, S.A. Chae, Y. Paik, S.H. Kwon, K.S. Lee, Y.E. Sung, H. Kim, Angew. Chem. Int. Ed. Engl., 50 (2011) 2270-2274.

[26] H. Wang, Z. Jusys, R.J. Behm, J. Power Sources, 154 (2006) 351-359.

[27] K. Taneda, Y. Yamazaki, Electrochim. Acta, 52 (2006) 1627–1631.

[28] Y. Katayanagi, Y. Yamazaki, Electrochemistry, 78 (2010) 976-981.

[29] F.C. Simoes, D.M. dos Anjos, F. Vigier, J.M. Leger, F. Hahn, C. Coutanceau, E.R. Gonzalez, G. Tremiliosi, A.R. de Andrade, P. Olivi, K.B. Kokoh, J. Power Sources, 167 (2007) 1.

[30] S. Ramachandran, U. Stimming, Energy Environ. Sci., 8 (2015) 3313-3324.

[31] N. Nakagawa, Y. Kaneda, M. Wagatsuma, T. Tsujiguchi, J. Power Sources, 199 (2012) 103.

[32] J.M. Jin, T. Sheng, X. Lin, R. Kavanagh, P. Hamer, P.J. Hu, C. Hardacre, A. Martinez-Bonastre, J. Sharman, D. Thompsett, W.F. Lin, Phys. Chem. Chem. Phys., 16 (2014) 9432-9440.

[33] D.D. James, P.G. Pickup, Electrochim. Acta, 55 (2010) 3824-3829.

[34] P. Majidi, P.G. Pickup, Electrochim. Acta, 182 (2015) 856–860.

[35] P. Majidi, R.M. Altarawneh, N.D.W. Ryan, P.G. Pickup, Electrochim. Acta, 199 (2016) 210-217.

[36] A. Ghumman, G. Li, D.V. Bennett, P. Pickup, J. Power Sources, 194 (2009) 286-290.

[37] Y. Liu, S.-F. Zhao, S.-X. Guo, A.M. Bond, J. Zhang, J. Am. Chem. Soc., 138 (2016) 2617-2628.

[38] L. Huang, E.G. Sorte, S.G. Sun, Y.Y.J. Tong, Chem. Commun., 51 (2015) 8086-8088.

[39] K. Alayavalli, D.L. Bourell, Rapid Prototyping Journal, 16 (2010) 268-274.

[40] C. Song, P.G. Pickup, J. Appl. Electrochem, 34 (2004) 1065-1070.

[41] A. Scheithauer, E. von Harbou, H. Hasse, T. Gruetzner, C. Rijksen, D. Zollinger, W.R. Thiel, AlChE J., 61 (2015) 177-187.

[42] S. Sun, M.C. Halseid, M. Heinen, Z. Jusys, R.J. Behm, J. Power Sources, 190 (2009) 2-13.

[43] V. Rao, C. Cremers, U. Stimming, L. Cao, S.G. Sun, S.Y. Yan, G.Q. Sun, Q. Xin, J. Electrochem. Soc., 154 (2007) B1138-B1147.

[44] D.D. James, D.V. Bennett, G.C. Li, A. Ghumman, R.J. Helleur, P.G. Pickup, Electrochem. Commun., 11 (2009) 1877-1880.

[45] R. Kavanagh, X.M. Cao, W.F. Lin, C. Hardacre, P. Hu, Angew. Chem. Int. Ed. Engl., 51 (2012) 1572-1575.

[46] Y.X. Wang, Y.J. Mi, N. Redmon, J. Holiday, J. Phys. Chem. C, 114 (2010) 317.

[47] Z.F. Xu, Y. Wang, Journal of Physical Chemistry C, 115 (2011) 20565-20571.

[48] S.E. Evarts, I. Kendrick, B.L. Wallstrom, T. Mion, M. Abedi, N. Dimakis, E.S. Smotkin, ACS Catalysis, 2 (2012) 701-707.

[49] H.F. Wang, Z.P. Liu, J. Am. Chem. Soc., 130 (2008) 10996-11004.

[50] J. Mann, N. Yao, A.B. Bocarsly, Langmuir, 22 (2006) 10432.

[51] A. Kowal, M. Li, M. Shao, K. Sasaki, M.B. Vukmirovic, J. Zhang, N.S. Marinkovic, P. Liu, A.I. Frenkel, R.R. Adzic, Nature Materials, 8 (2009) 325.

[52] E.A. Baranova, A. Tavasoli, T. Amir, Electrocatalysis, 2 (2011) 89.

[53] W.X. Du, Q. Wang, D. Saxner, N.A. Deskins, D. Su, J.E. Krzanowski, A.I. Frenkel, X.W. Teng, J. Amer. Chem. Soc, 133 (2011) 15172.

[54] J.C. Castro, M.H.M.T. Assumpcao, R.F.B. de Souza, E.V. Spinace, A.O. Neto, Electrocatalysis, 4 (2013) 159.

[55] M. Li, D.A. Cullen, K. Sasaki, N.S. Marinkovic, K. More, R.R. Adzic, J. Amer. Chem. Soc, 135 (2013) 132.

[56] L.A. Soares, C. Morais, T.W. Napporn, K.B. Kokoh, P. Olivi, J. Power Sources, 315 (2016) 47-55.

[57] D.D. James, P.G. Pickup, Electrochim. Acta, 78 (2012) 274-278.

[58] J. Seweryn, A. Lewera, Appl. Catal. B Environ, 144 (2014) 129.